EUROPEAN ORGANIZATION FOR NUCLEAR RESEARCH

CERN-EP/2003-019
April 7, 2003

Measurement of Branching Fractions of τ Hadronic Decays

The L3 Collaboration

Abstract

Using data collected with the L3 detector at LEP at the Z peak, the branching fractions of the τ lepton into the hadronic final states, $h^- n\pi^0\nu$ ($n = 0, 1, 2, \geq 3$) and $h^- h^+ h^- n\pi^0\nu$ ($n = 0, 1, \geq 2$), where $h^\pm$ denotes a charged hadron, are measured to be:

$$
\begin{array}{lrrrrrl}
\mathcal{B}(h^-\nu) & = & 12.09 & \pm & 0.12 & \pm & 0.10\ \% \\
\mathcal{B}(h^-\pi^0\nu) & = & 25.89 & \pm & 0.16 & \pm & 0.10\ \% \\
\mathcal{B}(h^-2\pi^0\nu) & = & 9.10 & \pm & 0.15 & \pm & 0.13\ \% \\
\mathcal{B}(h^- \geq 3\pi^0\nu) & = & 1.35 & \pm & 0.11 & \pm & 0.11\ \% \\
\mathcal{B}(h^-h^+h^-\nu) & = & 9.15 & \pm & 0.11 & \pm & 0.11\ \% \\
\mathcal{B}(h^-h^+h^-\pi^0\nu) & = & 4.81 & \pm & 0.12 & \pm & 0.08\ \% \\
\mathcal{B}(h^-h^+h^- \geq 2\pi^0\nu) & = & 0.66 & \pm & 0.08 & \pm & 0.04\ \% \ .
\end{array}
$$

The first uncertainty is statistical and the second systematic. The accuracy of these measurements is comparable to that of the current world average.

Submitted to the *European Physics Journal*

Introduction

The τ lepton is the only lepton massive enough to decay into hadrons, hence it provides a laboratory to study the weak hadronic current. Measurements of the branching fractions of the τ lepton into hadrons increase the precision of the determination of exclusive τ branching fractions. Among others, this improves the determination of the pion decay constant and the test of the vector current conservation. In this Letter we present new results for hadronic τ^- decays into one charged hadron h^- plus $n\pi^0$ ($n = 0, 1, 2, \geq 3$) and into three charged hadrons $h^-h^+h^-$ plus $n\pi^0$ ($n = 0, 1, \geq 2$), where h^- stands for π^- or K^- [1)]. We follow the convention that τ decays containing neutral kaons are excluded.

These results supersede our previous measurement [1]. Other measurements were published by several experiments [2].

The data were collected with the L3 detector [3] at LEP running at centre-of-mass energies around the Z mass and correspond to an integrated luminosity of 92.6 pb^{-1}.

For efficiency studies, $\mathrm{e^+e^-} \to \tau^+\tau^-(\gamma)$ events are generated with the KORALZ Monte Carlo generator [4]. Background estimations are performed using the following Monte Carlo generators: BHAGENE [5] for $\mathrm{e^+e^-} \to \mathrm{e^+e^-}(\gamma)$, KORALZ for $\mathrm{e^+e^-} \to \mu^+\mu^-(\gamma)$, JETSET [6] for $\mathrm{e^+e^-} \to \mathrm{q\bar{q}}(\gamma)$ and DIAG36 [7] for $\mathrm{e^+e^-} \to \mathrm{e^+e^-f\bar{f}}$, where $\mathrm{f\bar{f}}$ denotes a $\mathrm{e^+e^-}$, $\mu^+\mu^-$, $\tau^+\tau^-$ or $\mathrm{q\bar{q}}$ pair.

The Monte Carlo events are simulated in the L3 detector using the GEANT program [8] which takes into account the effects of energy loss, multiple scattering and showering in the detector. Time dependent detector inefficiencies, as monitored during data taking, are also simulated.

Subdetector Efficiencies and Calibrations

The subdetector efficiencies are determined as described in Reference 9. Data samples from the processes $\mathrm{e^+e^-} \to \mathrm{e^+e^-}(\gamma)$, $\mathrm{e^+e^-} \to \mu^+\mu^-(\gamma)$, $\mathrm{e^+e^-} \to \mathrm{e^+e^-e^+e^-}$, $\mathrm{e^+e^-} \to \mathrm{e^+e^-}\mu^+\mu^-$ as well as muons originating from τ decays are used to determine the efficiency of each subdetector. These studies are performed for each data taking period separately.

A track in the central tracker (TEC) must have at least 25 out of the 62 possible hits, one or more hits in the innermost part of the chamber and must span over more than 40 anode wires. Its transverse momentum must be larger than 2 GeV. After rejecting tracks in the low resolution region adjacent to the anode, the track finding efficiency is found to be about 96%, almost independent of the track momentum. The double track resolution of the TEC is determined from data [10] to be about 500 μm and is reproduced in the detector simulation. Small differences between data and simulated events are considered as systematic uncertainties.

The efficiencies of the electromagnetic calorimeter (BGO) to detect an electromagnetic shower or a minimum ionising particle (MIP) are determined to be about 99% and 97%, respectively. The efficiency of the hadron calorimeter (HCAL) to detect a MIP is about 89%. The muon spectrometer track finding efficiency for muons crossing more than one layer of chambers is 74%.

These subdetector efficiencies are used to correct the Monte Carlo simulation of the detector response to the $\mathrm{e^+e^-} \to \tau^+\tau^-(\gamma)$ and background processes. The energy scales of the subdetectors are calibrated using control data samples [11]. The scales of the BGO and the HCAL

[1)] Charge conjugation is implied throughout this Letter

are verified to better than 0.5% and 1%, respectively.

Selection of $e^+e^- \to \tau^+\tau^-(\gamma)$ Events

Events stemming from the process $e^+e^- \to \tau^+\tau^-(\gamma)$ are characterised by two jets with low track and calorimetric cluster multiplicities. A jet may also consist of an isolated electron or muon. Their selection is the same as described in Reference 9. To ensure good track measurements only events in the barrel region of the detector are accepted by requiring $|\cos\theta_{thrust}| < 0.7$, where θ_{thrust} is the polar angle of the thrust axis determined from tracks and calorimetric clusters. The event multiplicity, defined as the sum of the number of tracks[2)] and neutral clusters, is required to be less than 10. Each event is divided into two hemispheres with respect to the plane orthogonal to the thrust axis. The main backgrounds arise from the $e^+e^- \to e^+e^-(\gamma)$, $e^+e^- \to \mu^+\mu^-(\gamma)$ and $e^+e^- \to q\bar{q}(\gamma)$ processes and two-photon interactions. They are suppressed by cuts on the total energy deposited in the detector, on the energy deposited in the BGO or on the momenta of possible muons.

A sample of 70016 $e^+e^- \to \tau^+\tau^-(\gamma)$ events is selected. The estimations of the efficiencies and background fractions are done separately for each data taking period. The average selection efficiency for $e^+e^- \to \tau^+\tau^-(\gamma)$ events inside the barrel region of the detector, estimated from Monte Carlo, is $78.8 \pm 0.2\%$.

The background fractions are estimated from Monte Carlo and listed in Table 1. Scale factors around unity are applied to improve the agreement with data. They are obtained from a comparison to control data samples [9].

The background from cosmic rays is estimated from the distribution of the distance of closest approach to the beam position using muons and found to be negligible.

Photon and π^0 Identification

Photon and π^0 identification is the basis of this analysis. Local energy deposits with narrow shower shape in the BGO, not matching to a track, are searched for. They are denoted as neutral clusters. Neutral clusters in the vicinity of a hadron track are identified by subtracting from the BGO energy deposit an averaged transverse hadronic shower profile, adjusted in amplitude to the wide hadronic shower around the impact point of the track in the BGO [12]. The remaining local maxima of the energy deposit are then compared to the shape of an electromagnetic shower and an estimator, χ^2_{em}, is calculated. Hadronic τ decays at LEP energy result in narrow jets leading to energy deposits from hadrons and π^0's in a small cone. Low energy π^0's decay into photons with an opening angle sufficiently large to form two separate electromagnetic showers in the BGO with an invariant mass close to the π^0 mass. For high π^0 energies, the angle between the photons becomes smaller than the spatial resolution of the BGO and the two showers merge into a single one with relatively high energy. Electromagnetic showers in the BGO may also be faked by split-offs of hadronic showers which must be rejected. These tend to be of low energy and at a larger distance from the hadronic shower. They are suppressed by requiring the energy of the neutral clusters to be larger than 500 MeV and the angle between the neutral cluster and the nearest track to be less than 17 degrees. Finally, a neural network is used to separate electromagnetic showers and remaining split-off deposits from hadronic showers. The input variables for the neural network are: the energy and the mass of the neutral cluster,

[2)] Tracks from K^0_S are not counted in the track multiplicity [9].

where the mass is obtained by a fit to the shower profile assuming that the shower is originated by two photons, the invariant mass of the nearest track with the neutral cluster, the angle between the track and the neutral cluster and the value of χ^2_{em}. If a second neutral cluster is present a fit which constrains the invariant mass of the two neutral clusters to the π^0 mass is performed and its χ^2 is also fed into the neural network. The output of the neural network, $\mathcal{P}_{em}$, is interpreted as the probability of a neutral cluster to be of electromagnetic nature. Its distribution is shown in Figure 1a. The predictions for electromagnetic and split-off neutral clusters are well separated by the network and their sum is in very good agreement with the data.

A second neural network is trained to separate photons and unresolved π^0's. For this purpose, two training samples are selected from $e^+e^- \to \tau^+\tau^-(\gamma)$ data with enriched $\tau \to \rho\nu$ decays. The first sample must contain one neutral cluster and one track, with an invariant mass corresponding to the mass of the ρ meson. The neutral cluster is assumed to be an unresolved π^0. For the second sample, one track and two neutral clusters are required with an invariant mass compatible with the mass of the ρ meson. These neutral clusters are considered as photons. The input variables to the neural network are the energies of the neutral clusters, the value of χ^2_{em}, the invariant mass of the nearest track and the neutral cluster and the mass of the neutral cluster.

The neural network is applied to the total sample of $e^+e^- \to \tau^+\tau^-(\gamma)$ events. The output, shown in Figure 1b, represents the probability $\mathcal{P}_{\pi^0}$ of a neutral cluster to be a π^0. The separation power of the network is verified by selecting a photon sample by requiring $\mathcal{P}_{em} > 0.3$ and $\mathcal{P}_{\pi^0} < 0.3$ and calculating the invariant mass of the two clusters shown in Figure 1c. A clear peak at the mass of π^0 is observed with a negligible background.

Photons can also convert in the material inside the TEC giving additional tracks. These are identified as described in Reference 9 and their tracks and energy deposits in BGO are rejected from the event.

Rejection of τ Decays into Leptons and Neutral Kaons

The decays $\tau^- \to e^-\bar{\nu}_e\nu_\tau$ and $\tau^- \to \mu^-\bar{\nu}_\mu\nu_\tau$ are identified [13] and rejected from the sample. An electron is characterised by an energy deposit in the BGO matched with a TEC track. The shower shape must be consistent with an electromagnetic one. A muon is identified as a track in the muon chambers with energy deposits in the calorimeters consistent with a MIP. In regions without spectrometer coverage, a TEC track pointing to a MIP signature in the calorimeters is recognised as a muon.

In addition, τ decays into neutral kaons are rejected. They are identified as described in Reference 14. One TEC track originating from the interaction region is required. The energy deposit in the HCAL matched to this track is compared to the expectation for a hadron with a measured momentum p_{TEC}. The difference ΔE_{HCAL} between the observation and expectation tends to be large for hadronic τ decays containing neutral kaons. The quantity $\Delta E_{\mathrm{HCAL}}/\sqrt{p_{TEC}}$, shown in Figure 1d, must be larger than $3\sqrt{\mathrm{GeV}}$. In addition, the hadronic shower must be distributed to the deeper layers of the HCAL and the cosine of the angle α between the track and the shower must satisfy $0.9 < \cos\alpha < 0.9994$. With these cuts about 50% of the $\tau \to K^0X\nu$ decays are identified and rejected from the sample. The remaining ones are treated as background.

Analysis of 1-prong Hadronic τ Decays

To select 1-prong hadronic τ decays, one track is required in the corresponding hemisphere. The fraction of the decay modes $h^-\nu$, $h^-\pi^0\nu$, $h^-2\pi^0\nu$ and $h^- \geq 3\pi^0\nu$ is then obtained using a neural network approach.

Several networks are prepared whose input variables are: the total energies deposited in the BGO and HCAL in the corresponding hemisphere, the energies of the neutral clusters, the values of $\mathcal{P}_{em}$ and $\mathcal{P}_{\pi^0}$ and the invariant masses of all combinations of neutral clusters and of neutral clusters and the charged particle. For each τ decay channel, a large Monte Carlo sample is used to train the neural networks. The first network, denoted as NN_h, is trained using $h^-\nu$ decays as signal and all other channels as background. The second network, denoted as $NN_{h\pi^0}$, is trained using $h^-\pi^0\nu$ decays as the signal, and $h^-2\pi^0\nu$ and $h^- \geq 3\pi^0\nu$ decays as background. The last network, denoted as $NN_{h3\pi^0}$, is trained using $h^- \geq 3\pi^0\nu$ decays as signal, and $h^-2\pi^0\nu$ as background. The distributions of the outputs from NN_h, $NN_{h\pi^0}$ and $NN_{h3\pi^0}$ networks are shown in Figures 2, 3 and 4, respectively, for data and Monte Carlo. The signals are well separated towards large values whereas events of the background lie in the low value region.

Analysis of 3-prong Hadronic τ Decays

To select 3-prong hadronic τ decays, three tracks are required. Two neural networks are used to distinguish the decay modes $h^-h^+h^-\nu$, $h^-h^+h^-\pi^0\nu$ and $h^-h^+h^- \geq 2\pi^0\nu$.

These neural networks, denoted as NN_{3h} and $NN_{3h2\pi^0}$, are trained using $h^-h^+h^-\nu$ and $h^-h^+h^- \geq 2\pi^0\nu$ Monte Carlo events, respectively, as signals and the other channels as background. Input variables are the total energy deposits in the BGO and HCAL in the corresponding hemisphere, the momenta of the tracks, the energies of the neutral clusters, the values of $\mathcal{P}_{em}$ and $\mathcal{P}_{\pi^0}$ and the invariant masses of all combinations of the neutral clusters and of the neutral clusters and the charged particles. The output distributions for NN_{3h} and $NN_{3h2\pi^0}$ are shown in Figures 5 and 6, respectively, for data and Monte Carlo.

Determination of Hadronic τ Decay Branching Fractions

The neural network output distributions are used to simultaneously determine the branching fractions of the τ 1-prong decays into final states with zero, one, two and three or more π^0's and the 3-prong decays into final states with zero, one or more than two π^0's. A likelihood function is defined as:

$$\mathcal{L} = \mathcal{L}_1 \times \mathcal{L}_3,$$

where

$$\begin{aligned} \mathcal{L}_1 &= \prod_i P_1(N^i_{obs},\ N^i_{exp}) \text{ and} \\ \mathcal{L}_3 &= \prod_i P_3(N^i_{obs},\ N^i_{exp}) \end{aligned}$$

are the likelihood functions for 1-prong and 3-prong hadronic decays. P_1 and P_3 are Poisson distributions. For 1-prong decays the index i runs over the bins in the space spanned by the

outputs of the neural networks NN_h, $NN_{h\pi^0}$ and $NN_{h3\pi^0}$ and for 3-prong decays over the bins in the space of the neural networks NN_{3h} and $NN_{3h2\pi^0}$. N^i_{obs} is the number of τ's observed in the i-th bin, and N^i_{exp} is:

$$N^i_{exp} = N_\tau \sum_{j=1,7} \mathcal{B}(j)\varepsilon^{ij} + N^i_{bg},$$

where N_τ is the total number of τ decays in the barrel, as obtained from the measured cross section, and $\mathcal{B}(j)$ is the branching fraction of the decay channel j, with j running over all considered τ decays. The quantity ε^{ij} represents the selection efficiency for the decay channel j in the i-th bin, and N^i_{bg} is the number of other τ decays as well as non-τ background events in the i-th bin. The results are:

$$\begin{array}{lrcl}
\mathcal{B}(h^-\nu) & = & 12.09 \pm 0.12\ \% \\
\mathcal{B}(h^-\pi^0\nu) & = & 25.89 \pm 0.16\ \% \\
\mathcal{B}(h^-2\pi^0\nu) & = & 9.10 \pm 0.15\ \% \\
\mathcal{B}(h^- \geq 3\pi^0\nu) & = & 1.35 \pm 0.11\ \% \\
\mathcal{B}(h^-h^+h^-\nu) & = & 9.15 \pm 0.11\ \% \\
\mathcal{B}(h^-h^+h^-\pi^0\nu) & = & 4.81 \pm 0.12\ \% \\
\mathcal{B}(h^-h^+h^- \geq 2\pi^0\nu) & = & 0.66 \pm 0.08\ \%,
\end{array}$$

where the uncertainty is statistical. The use of different or additional neural networks does not change these results. The correlations between the 1-prong modes and between the 3-prong modes are non negligible and are given in Table 2 together with the systematic correlations discussed below. The results include those correlations.

Systematic Uncertainties

Several possible sources of systematic uncertainties are investigated. They are discussed in the following and their effect on the measured branching fractions are detailed in Table 3.

The cuts to suppress the different background processes are varied within the resolution of the corresponding variable. The change in the branching fractions is assigned as a systematic uncertainty. The uncertainty of the non-τ background fractions in the $e^+e^- \to \tau^+\tau^-(\gamma)$ sample is obtained by varying each Monte Carlo background fraction by the statistical uncertainty of its scale factor derived from control data [9]. The uncertainties on the cross sections of the background processes are also taken into account.

The criteria to identify τ decays into electrons, muons and kaons are varied within the resolution of the selection variables and the change of the branching fractions is assigned as systematic uncertainty.

The track efficiency is varied within its statistical error of 0.25% obtained from control data. The effect of the double track resolution is treated as in Reference 9. The criteria applied to identify neutral clusters are varied within the resolution of the corresponding variables. The energy scale uncertainty of each subdetector which is obtained from data, is varied within its statistical uncertainty. The systematic uncertainty from photon conversions is obtained by varying the estimated fraction of photon conversion tracks by its statistical error as determined from data.

The effect of nuclear interaction in the material between the beam pipe and the TEC is studied with samples of $e^+e^- \to \tau^+\tau^-(\gamma)$ events and the uncertainty in the modeling is found to be negligible.

The Monte Carlo generation of $\pi^-\pi^0\pi^0\nu$ and $\pi^-\pi^+\pi^-\nu$ decays is based on the KS model [15]. A more model independent analysis [16] revealed that the dominant W_A structure function is underestimated by this model. A reweighting of the Monte Carlo events is then performed using the measured W_A structure function. This implies a small shift of the branching fractions $\mathcal{B}(h^-2\pi^0\nu)$ and $\mathcal{B}(h^-h^+h^-\nu)$ included in the values quoted above. Half of these shifts is assigned as modeling uncertainty. The systematic uncertainty from minor discrepancies between neural network distributions for data and Monte Carlo is estimated by reweighting the Monte Carlo distributions so to enforce agreement with the data. Finally, the uncertainty from the Monte Carlo statistics is also considered.

The correlations between systematic uncertainties are estimated performing a large number of Monte Carlo experiments with variations of the relevant parameters around their central values. The covariance matrix obtained is added to the statistical one and the result is given in Table 2.

Conclusion

The branching fractions of the hadronic τ decays are measured with the L3 detector at LEP using a neural network approach. The results obtained by fitting the neural network outputs for each decay channel are:

$$
\begin{array}{lrrcrcl}
\mathcal{B}(h^-\nu) & = & 12.09 & \pm & 0.12 & \pm & 0.10\ \% \\
\mathcal{B}(h^-\pi^0\nu) & = & 25.89 & \pm & 0.16 & \pm & 0.10\ \% \\
\mathcal{B}(h^-2\pi^0\nu) & = & 9.10 & \pm & 0.15 & \pm & 0.13\ \% \\
\mathcal{B}(h^- \geq 3\pi^0\nu) & = & 1.35 & \pm & 0.11 & \pm & 0.11\ \% \\
\mathcal{B}(h^-h^+h^-\nu) & = & 9.15 & \pm & 0.11 & \pm & 0.11\ \% \\
\mathcal{B}(h^-h^+h^-\pi^0\nu) & = & 4.81 & \pm & 0.12 & \pm & 0.08\ \% \\
\mathcal{B}(h^-h^+h^- \geq 2\pi^0\nu) & = & 0.66 & \pm & 0.08 & \pm & 0.04\ \% \ .
\end{array}
$$

The first uncertainty is statistical and the second systematic. These values are in agreement with the current world averages [17] and are of comparable accuracy.

References

[1] L3 Collab., M. Acciarri *et al.*, Phys. Lett. **B 345** (1995) 93.

[2] ALEPH Collab., D. Decamp *et al.*, Z. Phys. **C 54** (1992) 211; CLEO Collab., M. Procario *et al.*, Phys. Rev. Lett. **70** (1993) 1207; CLEO Collab., M. Artuso *et al.*, Phys. Rev. Lett. **72** (1994) 3762; CLEO Collab., R. Balest *et al.*, Phys. Rev. Lett. **75** (1995) 3809; OPAL Collab., R. Akers *et al.*, Z. Phys. **C 68** (1995) 555; ALEPH Collab., D. Buskulic *et al.*, Z. Phys. **C 70** (1996) 579; CLEO Collab., A. Anastassov *et al.*, Phys. Rev. **D 55** (1997) 2559; CLEO Collab., A. Anastassov *et al.*, Phys. Rev. **D 58** (1998) 119903; OPAL Collab., K. Ackerstaff *et al.*, Eur. Phys. J. **C 4** (1998) 193.

[3] L3 Collab., B. Adeva *et al.*, Nucl. Instr. Meth. **A 289** (1990) 35; J.A. Bakken *et al.*, Nucl. Instr. Meth. **A 275** (1989) 81; O. Adriani *et al.*, Nucl. Instr. Meth. **A 302** (1991) 53; B. Adeva *et al.*, Nucl. Instr. Meth. **A 323** (1992) 109; K. Deiters *et al.*, Nucl. Instr. Meth. **A 323** (1992) 162; M. Chemarin *et al.*, Nucl. Instr. Meth. **A 349** (1994) 345; M. Acciarri *et al.*, Nucl. Instr. Meth. **A 351** (1994) 300.

[4] S. Jadach, B. F. L. Ward and Z. Wąs, Comp. Phys. Comm. **79** (1994) 503.

[5] J.H. Field, Phys. Lett. **B 323** (1994) 432; J.H. Field and T. Riemann, Comp. Phys. Comm **94** (1996) 53.

[6] T. Sjöstrand, Comp. Phys. Comm. **39** (1986) 347; T. Sjöstrand and M. Bengtsson, Comp. Phys. Comm. **43** (1987) 367.

[7] F.A. Berends, P.H. Daverfeldt and R. Kleiss, Nucl. Phys. **B 253** (1985) 441.

[8] R. Brun *et al.*, Preprint CERN DD/EE/84-1 (1984), revised September 1987.
The GHEISHA program (H. Fesefeldt, RWTH Aachen Report PITHA 85/02, 1985) is used to simulate hadronic interactions.

[9] L3 Collab., P. Achard *et al.*, Phys. Lett. **B 519** (2001) 189.

[10] F. Beissel *et al.*, Nucl. Instr. Meth. **A 332** (1993) 33.

[11] L3 Collab., M. Acciarri *et al.*, Phys. Lett. **B 429** (1998) 387.

[12] L3 Collab., O. Adriani *et al.*, Phys. Lett. **B 294** (1992) 466.

[13] L3 Collab., M. Acciarri *et al.*, Phys. Lett. **B 507** (2001) 47.

[14] L3 Collab., M. Acciarri *et al.*, Phys. Lett. **B 352** (1995) 487.

[15] J. H. Kühn and A. Santamaria, Z. Phys. **C 48** (1990) 445.

[16] CLEO Collab., T.E. Browder *et al.*, Phys. Rev. **D 61** (2000) 052004.

[17] K. Hagiwara *et al.*, Phys. Rev. **D 66** (2002) 010001.

The L3 Collaboration:

P.Achard,[20] O.Adriani,[17] M.Aguilar-Benitez,[24] J.Alcaraz,[24] G.Alemanni,[22] J.Allaby,[18] A.Aloisio,[28] M.G.Alviggi,[28] H.Anderhub,[46] V.P.Andreev,[6,33] F.Anselmo,[8] A.Arefiev,[27] T.Azemoon,[3] T.Aziz,[9] P.Bagnaia,[38] A.Bajo,[24] G.Baksay,[25] L.Baksay,[25] S.V.Baldew,[2] S.Banerjee,[9] Sw.Banerjee,[4] A.Barczyk,[46,44] R.Barillère,[18] P.Bartalini,[22] M.Basile,[8] N.Batalova,[43] R.Battiston,[32] A.Bay,[22] F.Becattini,[17] U.Becker,[13] F.Behner,[46] L.Bellucci,[17] R.Berbeco,[3] J.Berdugo,[24] P.Berges,[13] B.Bertucci,[32] B.L.Betev,[46] M.Biasini,[32] M.Biglietti,[28] A.Biland,[46] J.J.Blaising,[4] S.C.Blyth,[34] G.J.Bobbink,[2] A.Böhm,[1] L.Boldizsar,[12] B.Borgia,[38] S.Bottai,[17] D.Bourilkov,[46] M.Bourquin,[20] S.Braccini,[20] J.G.Branson,[40] F.Brochu,[4] J.D.Burger,[13] W.J.Burger,[32] X.D.Cai,[13] M.Capell,[13] G.Cara Romeo,[8] G.Carlino,[28] A.Cartacci,[17] J.Casaus,[24] F.Cavallari,[38] N.Cavallo,[35] C.Cecchi,[32] M.Cerrada,[24] M.Chamizo,[20] Y.H.Chang,[48] M.Chemarin,[23] A.Chen,[48] G.Chen,[7] G.M.Chen,[7] H.F.Chen,[21] H.S.Chen,[7] G.Chiefari,[28] L.Cifarelli,[39] F.Cindolo,[8] I.Clare,[13] R.Clare,[37] G.Coignet,[4] N.Colino,[24] S.Costantini,[38] B.de la Cruz,[24] S.Cucciarelli,[32] J.A.van Dalen,[30] R.de Asmundis,[28] P.Déglon,[20] J.Debreczeni,[12] A.Degré,[4] K.Dehmelt,[25] K.Deiters,[44] D.della Volpe,[28] E.Delmeire,[20] P.Denes,[36] F.DeNotaristefani,[38] A.De Salvo,[46] M.Diemoz,[38] M.Dierckxsens,[2] C.Dionisi,[38] M.Dittmar,[46] A.Doria,[28] M.T.Dova,[10,♯] D.Duchesneau,[4] M.Duda,[1] B.Echenard,[20] A.Eline,[18] A.El Hage,[1] H.El Mamouni,[23] A.Engler,[34] F.J.Eppling,[13] P.Extermann,[20] M.A.Falagan,[24] S.Falciano,[38] A.Favara,[31] J.Fay,[23] O.Fedin,[33] M.Felcini,[46] T.Ferguson,[34] H.Fesefeldt,[1] E.Fiandrini,[32] J.H.Field,[20] F.Filthaut,[30] P.H.Fisher,[13] W.Fisher,[36] I.Fisk,[40] G.Forconi,[13] K.Freudenreich,[46] C.Furetta,[26] Yu.Galaktionov,[27,13] S.N.Ganguli,[9] P.Garcia-Abia,[24] M.Gataullin,[31] S.Gentile,[38] S.Giagu,[38] Z.F.Gong,[21] G.Grenier,[23] O.Grimm,[46] M.W.Gruenewald,[16] M.Guida,[39] R.van Gulik,[2] V.K.Gupta,[36] A.Gurtu,[9] L.J.Gutay,[43] D.Haas,[5] D.Hatzifotiadou,[8] T.Hebbeker,[1] A.Hervé,[18] J.Hirschfelder,[34] H.Hofer,[46] M.Hohlmann,[25] G.Holzner,[46] S.R.Hou,[48] Y.Hu,[30] B.N.Jin,[7] L.W.Jones,[3] P.de Jong,[2] I.Josa-Mutuberría,[24] D.Käfer,[1] M.Kaur,[14] M.N.Kienzle-Focacci,[20] J.K.Kim,[42] J.Kirkby,[18] W.Kittel,[30] A.Klimentov,[13,27] A.C.König,[30] M.Kopal,[43] V.Koutsenko,[13,27] M.Kräber,[46] R.W.Kraemer,[34] A.Krüger,[45] A.Kunin,[13] P.Ladron de Guevara,[24] I.Laktineh,[23] G.Landi,[17] M.Lebeau,[18] A.Lebedev,[13] P.Lebrun,[23] P.Lecomte,[46] P.Lecoq,[18] P.Le Coultre,[46] J.M.Le Goff,[18] R.Leiste,[45] M.Levtchenko,[26] P.Levtchenko,[33] C.Li,[21] S.Likhoded,[45] C.H.Lin,[48] W.T.Lin,[48] F.L.Linde,[2] L.Lista,[28] Z.A.Liu,[7] W.Lohmann,[45] E.Longo,[38] Y.S.Lu,[7] C.Luci,[38] L.Luminari,[38] W.Lustermann,[46] W.G.Ma,[21] L.Malgeri,[20] A.Malinin,[27] C.Maña,[24] J.Mans,[36] J.P.Martin,[23] F.Marzano,[38] K.Mazumdar,[9] R.R.McNeil,[6] S.Mele,[18,28] L.Merola,[28] M.Meschini,[17] W.J.Metzger,[30] A.Mihul,[11] H.Milcent,[18] G.Mirabelli,[38] J.Mnich,[1] G.B.Mohanty,[9] G.S.Muanza,[23] A.J.M.Muijs,[2] B.Musicar,[40] M.Musy,[38] S.Nagy,[15] S.Natale,[20] M.Napolitano,[28] F.Nessi-Tedaldi,[46] H.Newman,[31] A.Nisati,[38] T.Novak,[30] H.Nowak,[45] R.Ofierzynski,[46] G.Organtini,[38] I.Pal,[43] C.Palomares,[24] P.Paolucci,[28] R.Paramatti,[38] G.Passaleva,[17] S.Patricelli,[28] T.Paul,[10] M.Pauluzzi,[32] C.Paus,[13] F.Pauss,[46] M.Pedace,[38] S.Pensotti,[26] D.Perret-Gallix,[4] B.Petersen,[30] D.Piccolo,[28] F.Pierella,[8] M.Pioppi,[32] P.A.Piroué,[36] E.Pistolesi,[26] V.Plyaskin,[27] M.Pohl,[20] V.Pojidaev,[17] J.Pothier,[18] D.Prokofiev,[33] J.Quartieri,[39] G.Rahal-Callot,[46] M.A.Rahaman,[9] P.Raics,[15] N.Raja,[9] R.Ramelli,[46] P.G.Rancoita,[26] R.Ranieri,[17] A.Raspereza,[45] P.Razis,[29] D.Ren,[46] M.Rescigno,[38] S.Reucroft,[10] S.Riemann,[45] K.Riles,[3] B.P.Roe,[3] L.Romero,[24] A.Rosca,[45] S.Rosier-Lees,[4] S.Roth,[1] C.Rosenbleck,[1] J.A.Rubio,[18] G.Ruggiero,[17] H.Rykaczewski,[46] A.Sakharov,[46] S.Saremi,[6] S.Sarkar,[38] J.Salicio,[18] E.Sanchez,[24] C.Schäfer,[18] V.Schegelsky,[33] H.Schopper,[47] D.J.Schotanus,[30] C.Sciacca,[28] L.Servoli,[32] S.Shevchenko,[31] N.Shivarov,[41] V.Shoutko,[13] E.Shumilov,[27] A.Shvorob,[31] D.Son,[42] C.Souga,[23] P.Spillantini,[17] M.Steuer,[13] D.P.Stickland,[36] B.Stoyanov,[41] A.Straessner,[18] K.Sudhakar,[9] G.Sultanov,[41] L.Z.Sun,[21] S.Sushkov,[1] H.Suter,[46] J.D.Swain,[10] Z.Szillasi,[25,℘] X.W.Tang,[7] P.Tarjan,[15] L.Tauscher,[5] L.Taylor,[10] B.Tellili,[23] D.Teyssier,[23] C.Timmermans,[30] Samuel C.C.Ting,[13] S.M.Ting,[13] S.C.Tonwar,[9] J.Tóth,[12] C.Tully,[36] K.L.Tung,[7] J.Ulbricht,[46] E.Valente,[38] R.T.Van de Walle,[30] R.Vasquez,[43] V.Veszpremi,[25] G.Vesztergombi,[12] I.Vetlitsky,[27] D.Vicinanza,[39] G.Viertel,[46] S.Villa,[37] M.Vivargent,[4] S.Vlachos,[5] I.Vodopianov,[25] H.Vogel,[34] H.Vogt,[45] I.Vorobiev,[34,27] A.A.Vorobyov,[33] M.Wadhwa,[5] Q.Wang,[30] X.L.Wang,[21] Z.M.Wang,[21] M.Weber,[1] P.Wienemann,[1] H.Wilkens,[30] S.Wynhoff,[36] L.Xia,[31] Z.Z.Xu,[21] J.Yamamoto,[3] B.Z.Yang,[21] C.G.Yang,[7] H.J.Yang,[3] M.Yang,[7] S.C.Yeh,[49] An.Zalite,[33] Yu.Zalite,[33] Z.P.Zhang,[21] J.Zhao,[21] G.Y.Zhu,[7] R.Y.Zhu,[31] H.L.Zhuang,[7] A.Zichichi,[8,18,19] B.Zimmermann,[46] M.Zöller.[1]

1 III. Physikalisches Institut, RWTH, D-52056 Aachen, Germany[§]
2 National Institute for High Energy Physics, NIKHEF, and University of Amsterdam, NL-1009 DB Amsterdam, The Netherlands
3 University of Michigan, Ann Arbor, MI 48109, USA
4 Laboratoire d'Annecy-le-Vieux de Physique des Particules, LAPP,IN2P3-CNRS, BP 110, F-74941 Annecy-le-Vieux CEDEX, France
5 Institute of Physics, University of Basel, CH-4056 Basel, Switzerland
6 Louisiana State University, Baton Rouge, LA 70803, USA
7 Institute of High Energy Physics, IHEP, 100039 Beijing, China[△]
8 University of Bologna and INFN-Sezione di Bologna, I-40126 Bologna, Italy
9 Tata Institute of Fundamental Research, Mumbai (Bombay) 400 005, India
10 Northeastern University, Boston, MA 02115, USA
11 Institute of Atomic Physics and University of Bucharest, R-76900 Bucharest, Romania
12 Central Research Institute for Physics of the Hungarian Academy of Sciences, H-1525 Budapest 114, Hungary[‡]
13 Massachusetts Institute of Technology, Cambridge, MA 02139, USA
14 Panjab University, Chandigarh 160 014, India.
15 KLTE-ATOMKI, H-4010 Debrecen, Hungary[$\mathcal{P}$]
16 Department of Experimental Physics, University College Dublin, Belfield, Dublin 4, Ireland
17 INFN Sezione di Firenze and University of Florence, I-50125 Florence, Italy
18 European Laboratory for Particle Physics, CERN, CH-1211 Geneva 23, Switzerland
19 World Laboratory, FBLJA Project, CH-1211 Geneva 23, Switzerland
20 University of Geneva, CH-1211 Geneva 4, Switzerland
21 Chinese University of Science and Technology, USTC, Hefei, Anhui 230 029, China[△]
22 University of Lausanne, CH-1015 Lausanne, Switzerland
23 Institut de Physique Nucléaire de Lyon, IN2P3-CNRS,Université Claude Bernard, F-69622 Villeurbanne, France
24 Centro de Investigaciones Energéticas, Medioambientales y Tecnológicas, CIEMAT, E-28040 Madrid, Spain[♭]
25 Florida Institute of Technology, Melbourne, FL 32901, USA
26 INFN-Sezione di Milano, I-20133 Milan, Italy
27 Institute of Theoretical and Experimental Physics, ITEP, Moscow, Russia
28 INFN-Sezione di Napoli and University of Naples, I-80125 Naples, Italy
29 Department of Physics, University of Cyprus, Nicosia, Cyprus
30 University of Nijmegen and NIKHEF, NL-6525 ED Nijmegen, The Netherlands
31 California Institute of Technology, Pasadena, CA 91125, USA
32 INFN-Sezione di Perugia and Università Degli Studi di Perugia, I-06100 Perugia, Italy
33 Nuclear Physics Institute, St. Petersburg, Russia
34 Carnegie Mellon University, Pittsburgh, PA 15213, USA
35 INFN-Sezione di Napoli and University of Potenza, I-85100 Potenza, Italy
36 Princeton University, Princeton, NJ 08544, USA
37 University of Californa, Riverside, CA 92521, USA
38 INFN-Sezione di Roma and University of Rome, "La Sapienza", I-00185 Rome, Italy
39 University and INFN, Salerno, I-84100 Salerno, Italy
40 University of California, San Diego, CA 92093, USA
41 Bulgarian Academy of Sciences, Central Lab. of Mechatronics and Instrumentation, BU-1113 Sofia, Bulgaria
42 The Center for High Energy Physics, Kyungpook National University, 702-701 Taegu, Republic of Korea
43 Purdue University, West Lafayette, IN 47907, USA
44 Paul Scherrer Institut, PSI, CH-5232 Villigen, Switzerland
45 DESY, D-15738 Zeuthen, Germany
46 Eidgenössische Technische Hochschule, ETH Zürich, CH-8093 Zürich, Switzerland
47 University of Hamburg, D-22761 Hamburg, Germany
48 National Central University, Chung-Li, Taiwan, China
49 Department of Physics, National Tsing Hua University, Taiwan, China
§ Supported by the German Bundesministerium für Bildung, Wissenschaft, Forschung und Technologie
‡ Supported by the Hungarian OTKA fund under contract numbers T019181, F023259 and T037350.
$\mathcal{P}$ Also supported by the Hungarian OTKA fund under contract number T026178.
♭ Supported also by the Comisión Interministerial de Ciencia y Tecnología.
♯ Also supported by CONICET and Universidad Nacional de La Plata, CC 67, 1900 La Plata, Argentina.
△ Supported by the National Natural Science Foundation of China.

Background source	Fraction [%]
$e^+e^- \to e^+e^-(\gamma)$	0.16 ± 0.02
$e^+e^- \to \mu^+\mu^-(\gamma)$	0.68 ± 0.01
$e^+e^- \to q\bar{q}(\gamma)$	1.59 ± 0.05
Two-photon interactions	0.16 ± 0.01

Table 1: The background fractions in the $e^+e^- \to \tau^+\tau^-(\gamma)$ event sample.

τ decays	$h^-\nu$	$h^-\pi^0\nu$	$h^-2\pi^0\nu$	$h^- \geq 3\pi^0\nu$	$h^-h^+h^-\nu$	$h^-h^+h^-\pi^0\nu$	$h^-h^+h^- \geq 2\pi^0\nu$
$h^-\nu$	1.000	−0.062	0.069	0.038	0.064	0.098	−0.007
$h^-\pi^0\nu$		1.000	−0.276	0.157	0.013	0.042	−0.039
$h^-2\pi^0\nu$			1.000	−0.523	−0.014	0.101	−0.073
$h^- \geq 3\pi^0\nu$				1.000	0.021	0.159	−0.091
$h^-h^+h^-\nu$					1.000	−0.044	0.197
$h^-h^+h^-\pi^0\nu$						1.000	−0.359
$h^-h^+h^- \geq 2\pi^0\nu$							1.000

Table 2: Correlation coefficients, including systematics, between the τ hadronic branching fractions.

Decay modes	$\tau^- \to h^-n\pi^0\nu$				$\tau^- \to h^-h^+h^-n\pi^0\nu$		
	$n=0$	$n=1$	$n=2$	$n \geq 3$	$n=0$	$n=1$	$n \geq 2$
$e^+e^- \to e^+e^-(\gamma)$	0.017	0.035	0.043	0.037	0.005	0.015	0.004
$e^+e^- \to \mu^+\mu^-(\gamma)$	0.013	0.030	0.055	0.022	0.004	0.003	0.002
$e^+e^- \to q\bar{q}(\gamma)$	0.004	0.026	0.042	0.063	0.055	0.026	0.029
Two-photon interactions	0.035	0.016	0.013	0.016	0.006	0.010	0.005
Leptonic τ decays	0.066	0.036	0.046	0.033	0.007	0.002	0.001
τ decays into K^0	0.025	0.016	0.016	0.012	0.004	0.001	<0.001
Track selection	0.023	0.013	0.031	0.038	0.065	0.057	0.025
Neutral cluster selection	0.008	0.026	0.021	0.018	0.008	0.007	0.002
Scale uncertainties	0.014	0.028	0.020	0.030	0.012	0.013	0.013
Photon conversions	0.004	0.008	0.021	0.023	0.005	0.001	<0.001
W_A modeling	0.001	0.013	0.065	0.011	0.039	0.003	0.001
Neural network	0.028	0.008	0.028	0.027	0.044	0.017	0.004
Monte Carlo statistics	0.041	0.061	0.035	0.013	0.043	0.032	0.013
Total	0.100	0.101	0.133	0.107	0.114	0.076	0.043

Table 3: Systematic uncertainties on the τ hadronic branching fractions, in %.

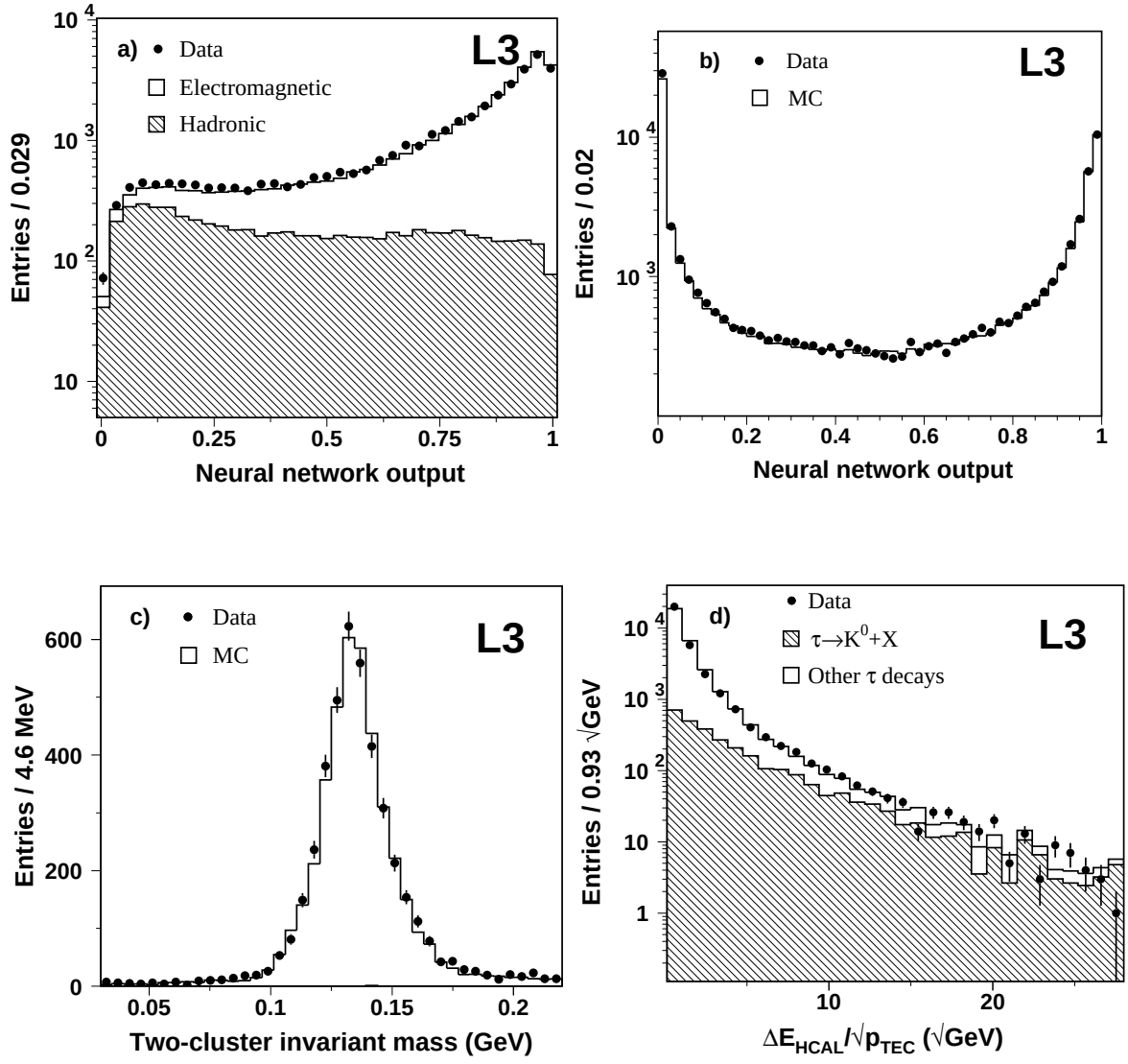

Figure 1: Distributions for data and Monte Carlo of: a) the output of the neural network used to discriminate electromagnetic showers from split-off deposits caused by hadronic showers. b) the output of the neural network used to discriminate photons from π^0's. The output peaks at large values for π^0's and at low values for photons. c) the invariant mass of two neutral clusters which have an output in a) above 0.3 and an output in b) below 0.3. d) the difference between the energy measured in ECAL and predicted from the track momentum p_{TEC}, divided by $\sqrt{p_{TEC}}$. The Monte Carlo distributions are normalised to the number of data events.

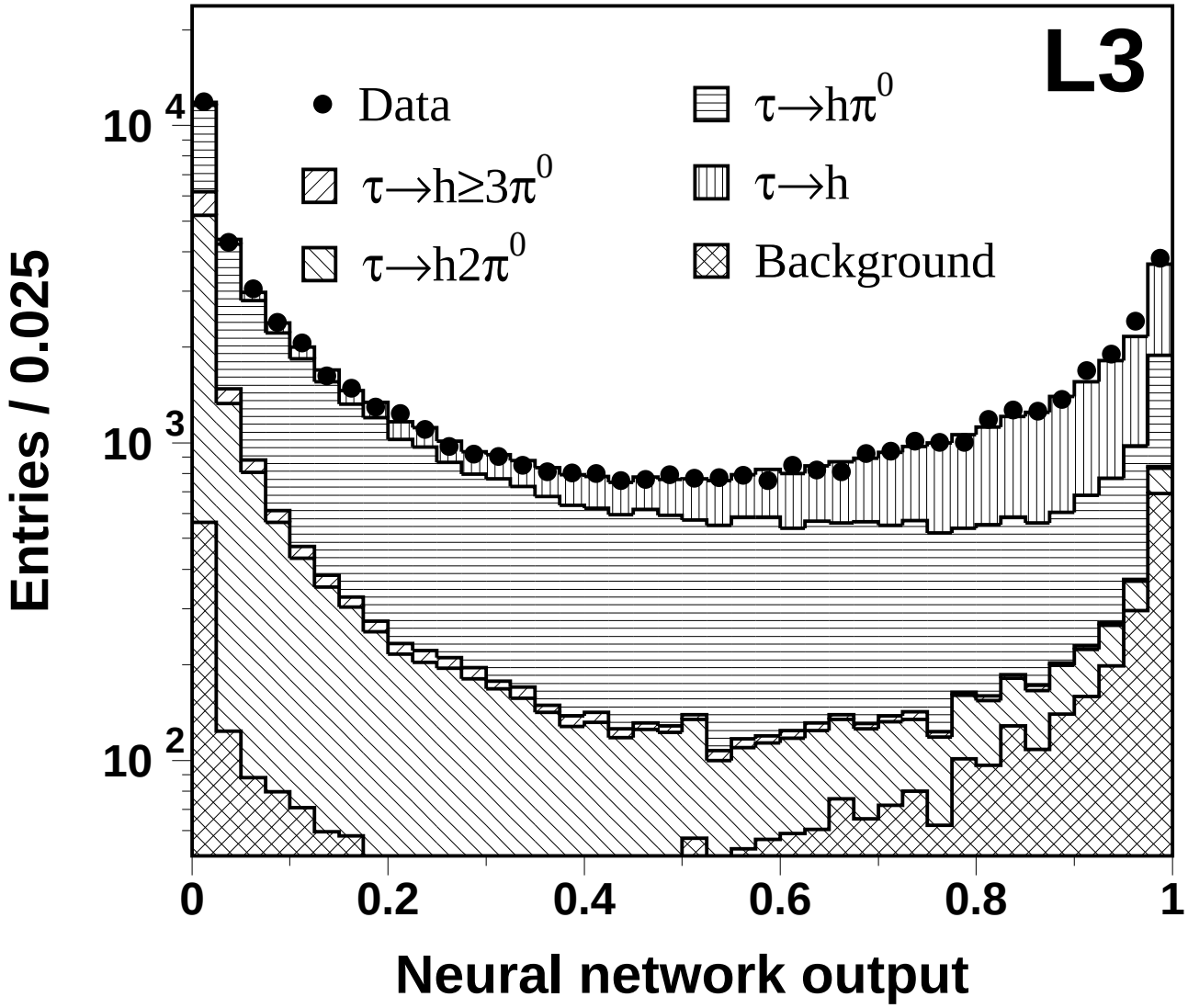

Figure 2: The distribution of the output of the neural network NN_h trained to identify $\tau^- \to h^-\nu$ decays. The Monte Carlo distributions are normalised to the number of data events using the measured τ branching fractions.

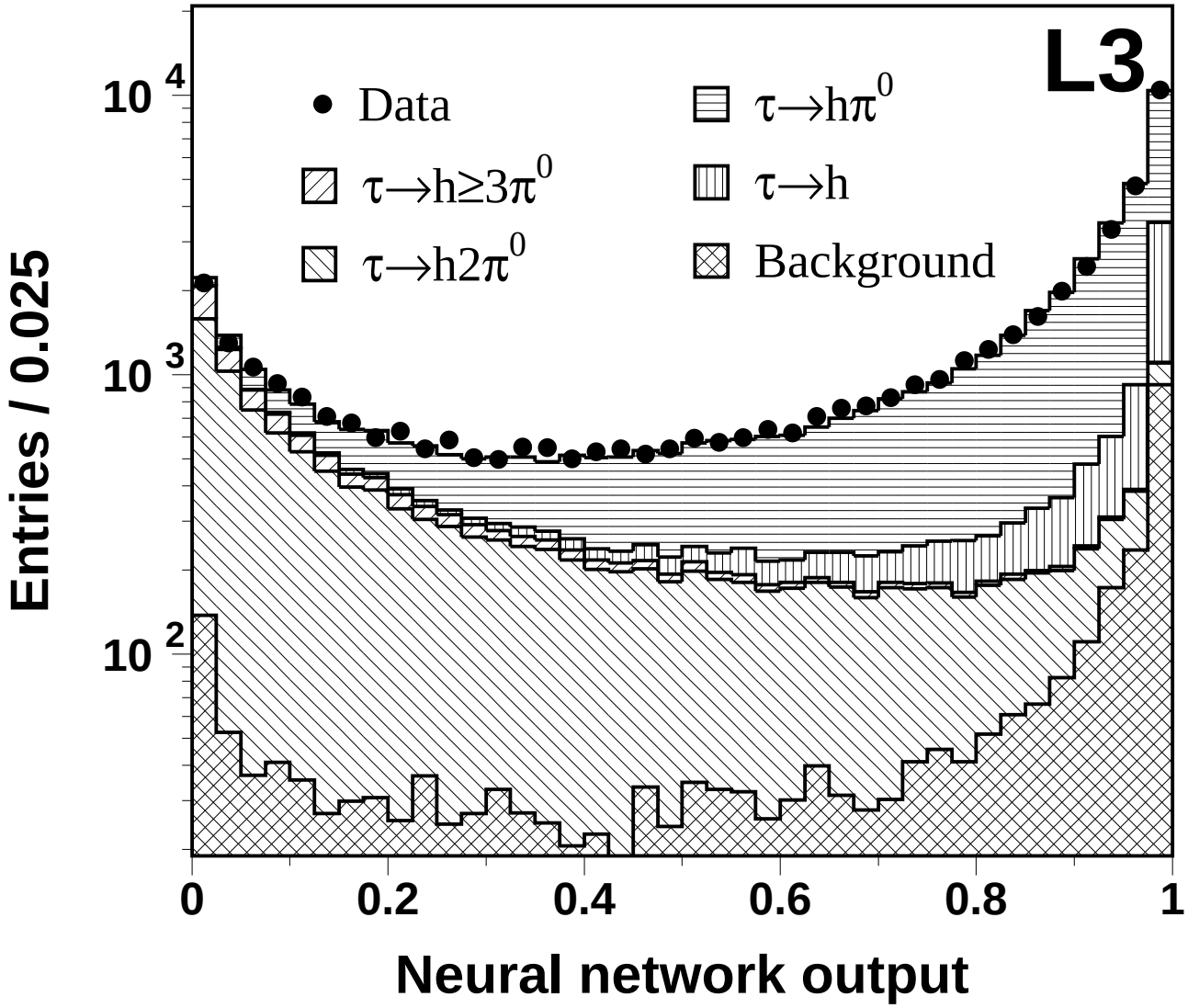

Figure 3: The distribution of the output of the neural network $NN_{h\pi^0}$ trained to identify $\tau^- \to h^-\pi^0\nu$ decays. The Monte Carlo distributions are normalised to the number of data events using the measured τ branching fractions.

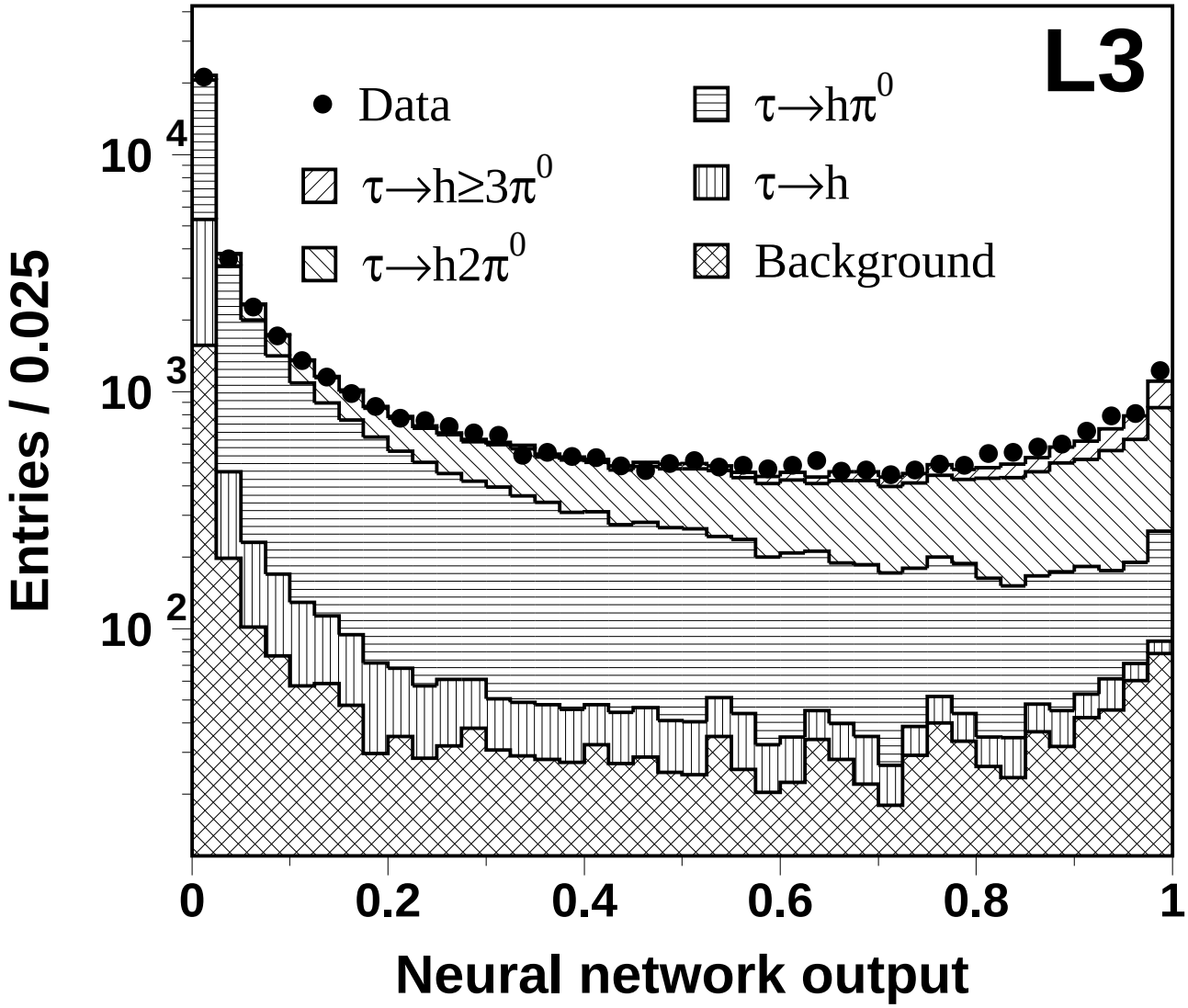

Figure 4: The distribution of the output of the neural network $NN_{h3\pi^0}$ trained to identify $\tau^- \to h^- \geq 3\pi^0\nu$ decays. The Monte Carlo distributions are normalised to the number of data events using the measured τ branching fractions.

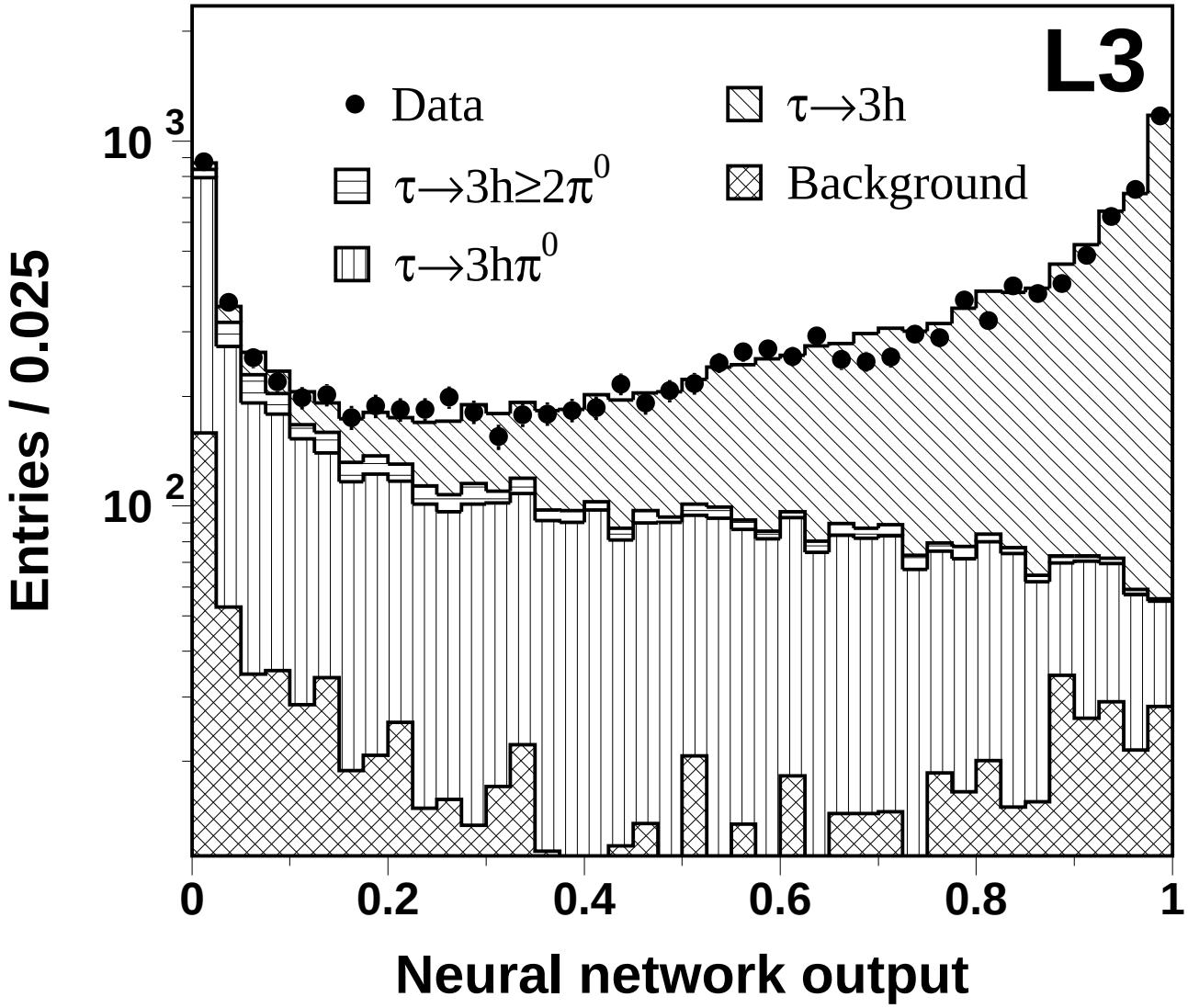

Figure 5: The distribution of the output of the neural network NN_{3h} trained to identify $\tau^- \to h^-h^+h^-\nu$ decays. The Monte Carlo distributions are normalised to the number of data events using the measured τ branching fractions.

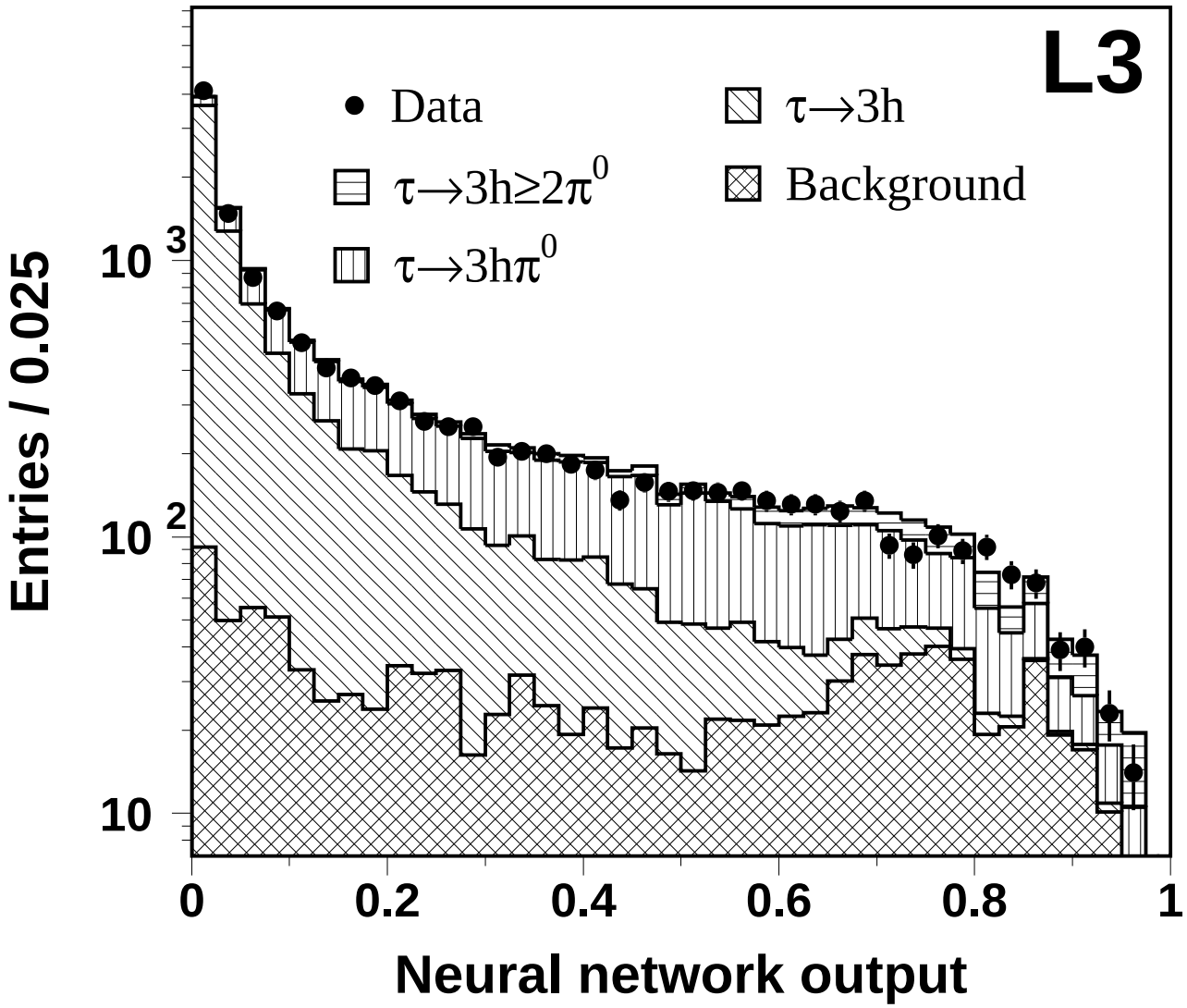

Figure 6: The distribution of the output of the neural network $NN_{3h2\pi^0}$ trained to identify $\tau^- \to h^-h^+h^- \geq 2\pi^0\nu$ decays. The Monte Carlo distributions are normalised to the number of data events using the measured τ branching fractions.